

Effect of Cr and Zr on the Tensile Creep Behavior of Al-5Fe Based Semisolid Alloys

BO LIU^{1,2}

1.—School of Naval Architecture and Electromechanical Engineering, Zhejiang Ocean University, Zhoushan 316022, People's Republic of China. 2.—e-mail: liubo@zjou.edu.cn

Determining the dominant creep mechanism is the key feature for design and development of Al-Fe alloys. The tensile creep behavior of Al₅Fe₄-Cu₂ZnMnMg alloy (AF1) and Al₅Fe₄Cu₂CrZnZrMnMg alloy (AF15) by prepared semisolid forming has been investigated. The results reveal that the steady-state creep rates of the AF1 and AF15 alloys are increased with increasing temperature and applied stress. The creep property of the AF15 alloy is slightly higher than that of the AF1 alloy. There is threshold stress during creep. The creep true stress exponent is close to 5. The creep mechanism of the alloys is controlled by the lattice diffusion of aluminum. The creep resistance of the AF15 alloy is significantly improved by adding a small amount of Cr and Zr elements. The reasons for the improved creep life of the AF15 alloy are discussed.

INTRODUCTION

Aluminum and its alloys, as a class of light materials, have been known to be suitable candidates possessing excellent castability, low density and good machinability. As with the Ni-based superalloys, the unit cell of aluminum is face centered cubic (fcc), whose close packed structure is more creep-resistant than a more open crystalline structure.¹ The main problem involved in using traditional aluminum alloys, however, is the drastic drop in their high-temperature mechanical properties and creep resistance with increasing the temperature to above 200°C.^{2,3} To address this deficiency, Al-Fe alloys as potential structural materials have been developed.^{4,5} Al-Fe alloys are believed to represent a promising candidate for applications at elevated temperatures.

Many reports on the creep behavior of Al-Fe alloys are mainly about Al-Fe-V-Si systems by means of rapid solidification technology, powder metallurgy or mechanical alloying.⁶⁻⁸ These alloys maintain their strength at high temperature and have good creep resistance. Especially if they have been reinforced with ceramic particulates, short fibers or whiskers, their creep properties will be enhanced further since those reinforcements increased the elastic modulus and could markedly improve the high-temperature strength of the

alloys.⁹ In addition, the creep behavior of Al-Fe alloys with low Fe have also been investigated.^{10,11} The creep resistance of the binary Al-Fe alloys was greatly improved with increasing Fe contents, which is attributed to the larger volume fraction of fine intermetallic particles pinned unevenly on the subgrain boundary, making the pinned subgrains unable to merge with the surrounding subgrains.¹¹

Attempts have been made to improve the mechanical properties such as creep resistance of Al alloys by adding a small amount of alloying elements for the formation of strengthening phases or the alteration feature of second phases as AlFe intermetallics.^{12,13} The addition of alloying elements may improve the mechanical properties of semisolid Al-5Fe-based alloys,¹⁴ but very few studies have paid attention to their creep behavior.

In this study, the tensile creep of the Al-5Fe-based semisolid alloys have been investigated. The creep parameters and creep deformation mechanism of the alloys have been estimated. The effect of Cr and Zr on the creep behavior of AF15 alloy has also been discussed.

EXPERIMENTAL DETAILS

Two kinds of Al-5Fe-based semisolid alloys were prepared for the tensile creep, and their chemical compositions were analyzed using an x-ray

fluorescence spectrometer and are listed in Table I. The alloy preparation process is described in detail in Ref. 4.

The creep specimens were cut from Al-5Fe-based semisolid alloy ingots. The cylindrical specimens with a dimension of 6 mm and a gauge length of 25 mm were placed in a heating furnace on an Andrade lever arm-type high-temperature creep-testing apparatus, with three thermocouples to prevent local overheating and to maintain the specimen at a uniform temperature, slowly heated to the target temperature and then held about 2 h before creep testing began. The creep strain generated by a constant-load device acting on the specimen was captured by a displacement indicator. The precision of the displacement indicator and the temperature controller were ± 0.01 mm and $\pm 1^\circ\text{C}$, respectively. Some samples were used for direct tensile rupture, another small part of the samples were kept for many tens of hours after achieving the steady-state creep stage (creep strain is about 2–3%) and then rapidly increased to a higher target temperature until the sample snapped. The experimental temperature and applied stress employed in the creep were in the ranges of 200–350°C and 30–100 MPa, respectively. The microstructures of the Al-5Fe-based alloy specimens were characterized by a Hitachi S-3400 N scanning electron microscope at an accelerating voltage of 15 kV.

RESULTS

The tensile creep curves of the Al-5Fe-based semisolid alloys are shown in Fig. 1. The tensile deformation of the alloys was increased with increasing the temperature and the applied stress. The creep durations of the alloys at different temperatures and applied stresses were used to assess the creep resistance, as shown in Table II. The steady-state creep rates were increased with increasing temperature and applied stress, while the creep durations decreased with increasing temperature and applied stress. The steady-state creep rates increased from 1.59×10^{-5} mm/s of AF1 alloy to 2.16×10^{-6} mm/s of AF15 alloy at the temperature of 250°C and stress of 100 MPa. With the applied stress increasing, the creep initial strain capacity of the alloys was increased and the decelerating creep stage was also shortened. With the creep temperature increasing, the decelerating creep stage of the alloys was obviously shortened from many tens of hours at 200°C to a couple of minutes. The durations of the AF1 and AF15 alloys

were increased to hundreds of hours at the temperature of 200°C and the applied stress of 100 MPa from many tens of hours at 250°C and 100 MPa.

It can be seen from Fig. 1 that the strain difference at high temperature was larger than that at low temperature. The strain difference under high stress surpassed that under low stress. The strain difference generated under high temperature and moderate stress exceeded those under large stress and low temperature. This indicated that the creep strain of the AF15 and AF1 alloys was controlled by stress at low temperatures, and varied with temperature at high temperatures. The creep strain was controlled by stress under high stress, and varied with temperature under low stress.

DISCUSSION

Creep Parameters

The relationship between the steady-state creep rate, $\dot{\epsilon}_s$, creep apparent stress exponent, n , and activation energy, Q_a , of a polycrystalline material can be expressed by the equation:¹⁵

$$\dot{\epsilon}_s = A\sigma^n \exp\left(-\frac{Q}{RT}\right) \quad (1)$$

where A is the structure-dependent constant, σ is the nominal normal stress, n is the apparent stress exponent determined by the deformation mechanism, Q_a is the creep apparent activation energy, R is the gas constant and T is the absolute temperature.

Figure 2a and b show the logarithmic relationship between $\dot{\epsilon}_s$ and σ at different temperatures, and Fig. 2c and d presents the relationship between $\ln \dot{\epsilon}_s$ and $1/T$ under different stresses of the AF15 and AF1 alloys, respectively. The apparent stress exponent n values of all the experimental alloys were from 6.78 to 7.65 and the apparent creep activation energy Q_a values from 207.39 kJ/mol to 229.79 kJ/mol for the AF1 and AF15 alloys, respectively.

Generally, the combination of different stress exponents and activation energies can determine the creep mechanism of materials.^{15,16} However, the apparent stress exponent n average values and the average apparent activation energies for the AF1 and AF15 alloys were 7.10 ± 0.19 and 220.60 ± 9.14 , and 7.13 ± 0.35 and 216.53 ± 3.19 , respectively, with these creep parameters being little different between the AF1 and AF15 alloys. The apparent activation energy decreased with

Table I. Chemical composition of semisolid formed Al-5Fe -based alloys (wt.%)

Alloy	Fe	Cu	Zn	Cr	Mn	Mg	Zr	Ti	B	Al
AF1	4.0–6.0	3.8–4.2	1.5–2.5	–	0.4–0.6	0.3–0.5	≤ 0.06	≤ 0.1	≤ 0.01	Bal.
AF15	4.5–5.5	4.0–4.5	0.5–1.5	1.8–2.1	0.5–0.6	0.3–0.5	0.25–0.35	≤ 0.1	≤ 0.01	Bal.

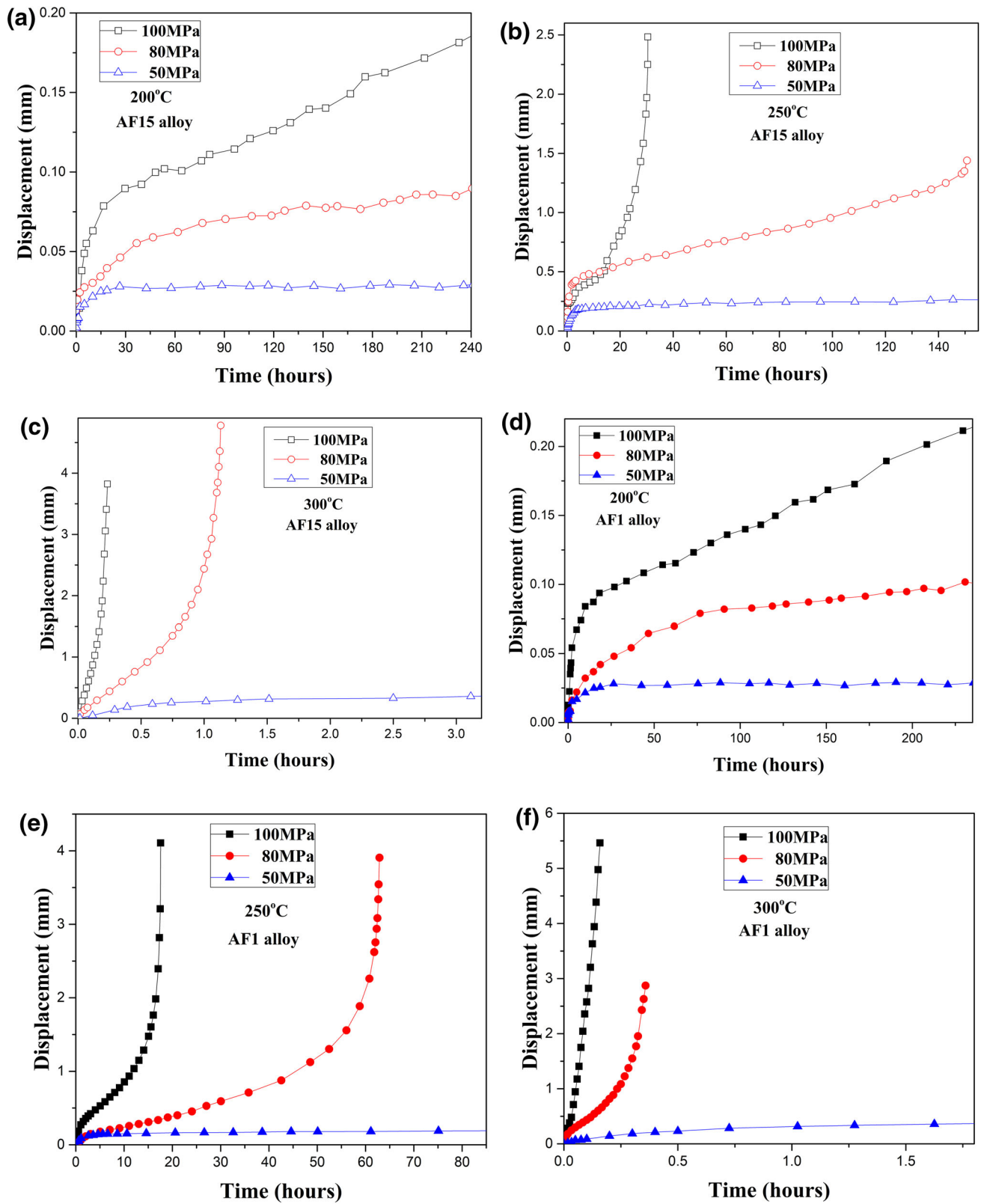


Fig. 1. Tensile creep curves of Al-5Fe-based semisolid alloys under different applied stresses and temperature for the AF15 alloy at 200°C (a), 250°C (b), 300°C (c) and for the AF1 alloy at 200°C (d), 250°C (e), 300°C (f).

Table II. Tensile creep duration of Al-5Fe -based semisolid alloys under various temperatures and applied stresses

Temperature (°C)	Applied strain (MPa)	AF1 alloy (h)	AF15 alloy (h)
200	100	> 250	> 523
250	100	17.6	36.7
	80	62.9	155.6
300	100	0.158	0.233
	80	0.36	1.13
	50	33.5	60.25
350	30	3.15	12.2

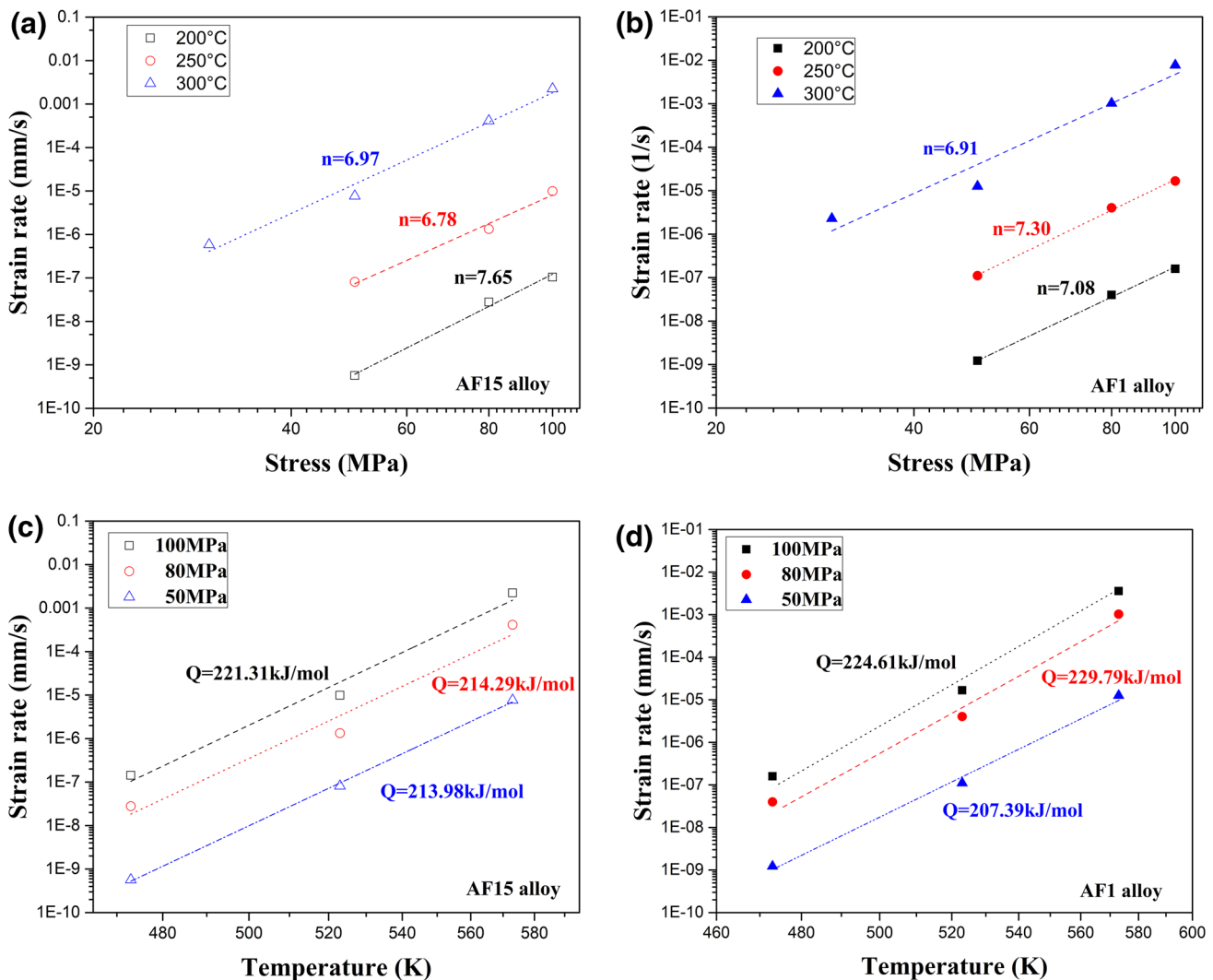


Fig. 2. The apparent stress exponent n of AF15 (a) and AF1 alloys (b) at different temperatures and the creep apparent activation energy Q_c of AF15 (c) and AF1 (d) at different stresses.

increasing the load, and the apparent activation energy of ~ 200 kJ/mol was higher than the lattice diffusion activation energy of aluminum of 142 kJ/mol.¹ This indicates that abnormal creep characteristics were present as compared to traditional aluminum materials, signifying that there

was an internal stress in the Al-5Fe-based semisolid alloys during tensile creep.

Threshold Stress and True Stress Exponents

When precipitates act as effective obstacles to dislocation motion,¹⁷ no appreciable creep can occur

at stresses below the threshold stress.^{15,18} Hence, the power law equation for steady-state creep in precipitate-strength alloys at a constant temperature can be written as:¹⁸

$$\dot{\epsilon}_{\min} = A'(\sigma - \sigma_{\text{th}})^{n_t} \quad (2)$$

where $\dot{\epsilon}_{\min}$ is the minimum creep rate, σ is the applied stress, σ_{th} is the creep threshold stress, A' (where $A' \neq A$) is a material constant, and nt (where $nt \neq n$) is the true stress exponent of the material.

At each deformation temperature, the linear relationship is satisfied between $\dot{\epsilon}_s$ and σ , and the corresponding stress is the threshold stress at this temperature when the strain rate is extrapolated to zero. The threshold stress of the Al-5Fe-based semisolid alloys at various temperatures were estimated by extrapolating from the $\dot{\epsilon}_s - \sigma$ curve. The most appropriate n value is the best linear fitting between $\dot{\epsilon}_s$ and σ , i.e. the R -squared value of the linear regression coefficient is the highest. The fitting of different n (such as $n = 2, 3, 5$ and 8) showed that the $n = 5$ linear relationship was the best, giving a threshold stress σ_{th} of 14.97 MPa, 19.53 MPa and 20.99 MPa for the AF1 alloy at 300°C, 250°C and 200°C, and of 17.76 MPa, 20.27 MPa and 22.41 MPa for the AF15 alloy at 300°C, 250°C and 200°C, respectively. The threshold stress decreased with increasing creep temperature for all the alloys. At equal temperature, the AF15 alloy showed higher threshold stress than the AF1 alloy for all the testing conditions, indicating the AF15 alloy had a stronger creep resistance than the AF1 alloy.

Figure 3 shows the plots of the steady-state creep rate, $\dot{\epsilon}$, against the effective stress ($\sigma - \sigma_{\text{th}}$) on a logarithmic scale with the slopes of the plots, giving the values of the true stress exponent n_t . The different true stress exponent refers to the diverse creep control mechanism.¹⁵ The true stress exponents of the Al-5Fe-based alloys were between 4.34 and 5.34 for all temperatures, while the average values of the AF1 and AF15 alloys were 4.88 ± 0.2 and 4.80 ± 0.5 , respectively. The small difference in n_t values for the AF1 and AF15 alloys and having both values near 5 indicates that the creep was governed by the high temperature climb controlled by lattice self-diffusion.¹⁹

Effect of Cr and Zr on Creep Life

Either the creep temperature increases under equal stress condition or, as the stress increases at equal temperatures, the creep rate of the Al-5Fe-based semisolid alloys was accelerated and the creep life was gradually shortened. The stress exponent and creep activation energy of the AF1 and AF15 alloys were little different, although the creep rupture life of the AF15 alloy was significantly higher than that of the AF1 alloy.

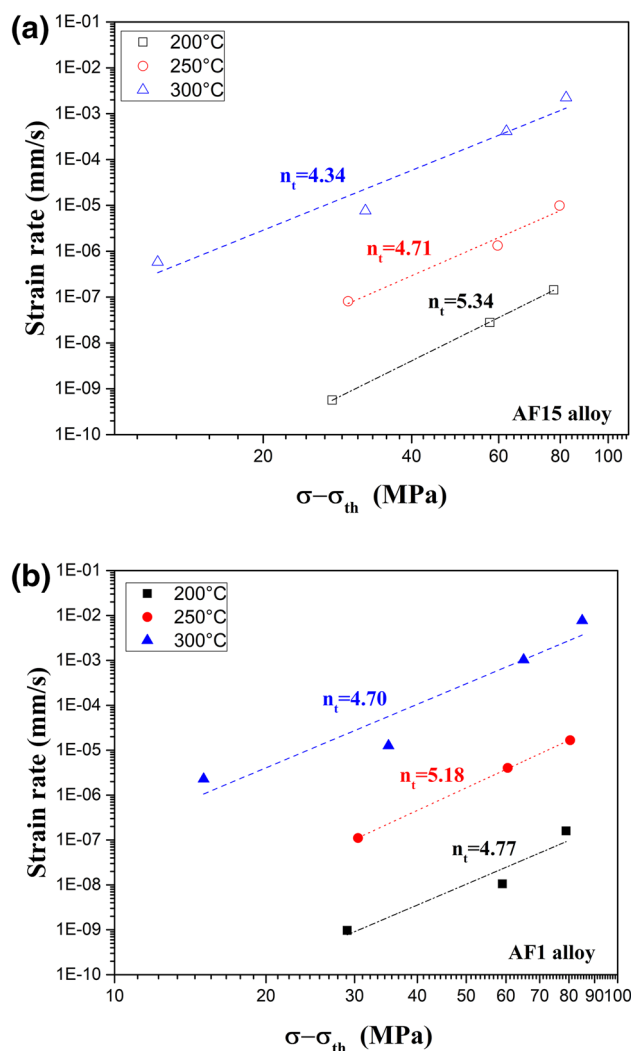


Fig. 3. The true stress exponent n_t of the AF15 (a) and AF1 alloys (b) at different temperatures.

Chromium added to the Al-5Fe semisolid alloy dissolved mainly in the $\text{Al}_{13}\text{Fe}_4$ phase. The resulting morphology of the $\text{Al}_{13}\text{Fe}_4$ phase with high Cr was a transformation from plate-like to lump-like or ring-like, and the density and thermal stability were higher than that without Cr or with lower Cr.^{14,20} Zirconium had formed the acicular Al_3Zr or the $\text{Al}_3(\text{ZrTi})$ phase in the alloy, in which most of these phases which germinated on the edge or at both ends of the iron-rich intermetallics could occupy the developing spaces of the AlFe phases and indirectly hinder the growth of Fe-bearing phases.¹⁴

Figure 4 depicts the creep rupture morphology of the Al-5Fe-based semisolid alloys under different experimental conditions. AF1 alloy belongs to the ductile intergranular fracture, in which the fracture surface was damaged and there were some dimples with varying sizes and depth, torn edges and an iron-rich phase. The dimples' interior had a distinct glide step. The dimples were actually composed of

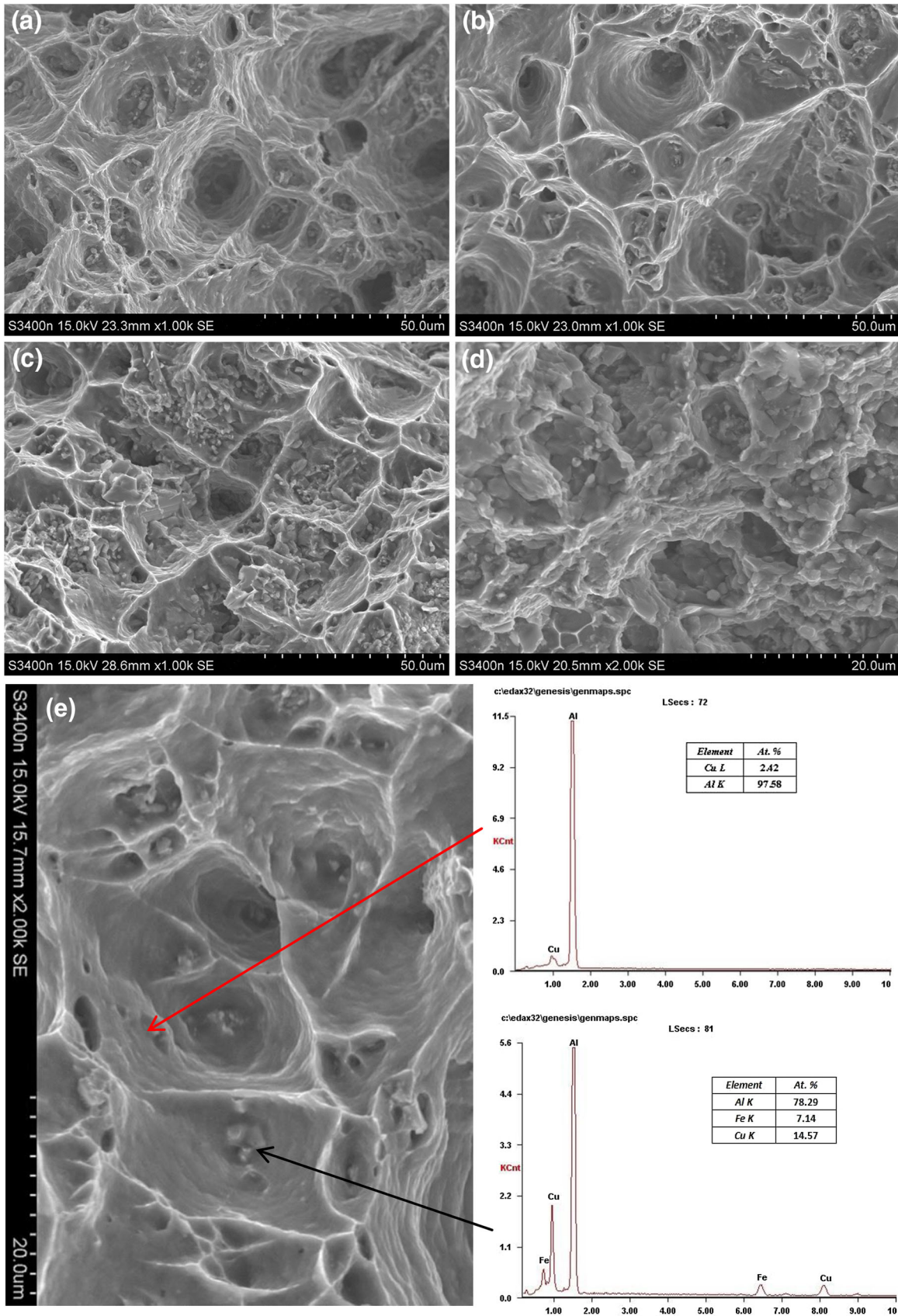


Fig. 4. The creep microstructure of the AF1 alloy (a) at 350°C for 30 MPa and (b) at 300°C for 80 MPa and of the AF15 alloy (c) at 300°C for 50 MPa (d) at 350°C for 30 MPa and (e) EDS of fracture of AF1 alloy for creep at 250°C and 80 MPa.

many small smooth platforms and had many secondary cracks. The torn edges were not very obvious, and a number of the $\text{Al}_7\text{Cu}_2\text{Fe}$ precipitated particles on the bottom were observed (Fig. 4e). Nevertheless, there were many tiny granular fragments on the fracture of the AF15 alloy, and there was not a smooth, bright cleavage plane between the grains, which should be the result of the intergranular fracture. There were also a few dimples on the fracture and many grains had ruptured along the crystal in the interior of the dimples unlike the interior of the dimple in the AF1 alloy which had smooth glide steps and many secondary cracks, indicating that the grain boundary sliding in the AF15 alloy was more difficult than in the AF1 alloy during creep. There were less potential crack sources in the AF15 alloy.

During the creep process, the Al-5Fe-based semisolid alloys cavitated easily on the grain boundaries. Either the dislocation accumulated on the grain boundaries and/or the $\text{AlFe}/\alpha\text{-Al}$ interfaces causing a discontinuity for strain made its inner free surface generate plentiful micro-holes, or, under the action of tension stress, a vast plastic deformation made the brittle iron-rich intermetallics fracture or disconnect from the matrix to form a hole in the $\text{AlFe}/\alpha\text{-Al}$ interface. Once the hole was formed, it would develop and concentrate, resulting in the formation of cracks.²¹ Under high stress creep, the hole at the trigeminal node in the grain boundary became wedge cracks which caused local grain boundary separation, and they interacted and interconnected resulting finally in rupturing.¹⁸ Under low stress, the hole nucleated on the grain boundary and/or the $\text{AlFe}/\alpha\text{-Al}$ interface and developed and merged to generate fractures.

For the AF15 alloy, many AlFe phases' morphology converted because of adding Cr and Zr, decreasing the source of cracks caused by stress concentration. Simultaneously, the development of AlZr compounds would also hinder the cracks developing at these places. Additionally, the quantity and genre of second phases in the AF15 alloy is more and more complex than those in the AF1 alloy, making the cavity also subject to greater resistance in the developing and merging process, and the crack growth was slower. Thus, the creep resistance of the AF15 alloy is higher and the creep life is more durable. The creep stress exponent and the activation energy of the AF15 and AF1 alloys were similar, although the lower forming probability of the micro-holes or cracks caused by reducing stress concentration because of forming more thermostable and more denser lump-like or ring-like AlFe phases with high Cr, could more effectively pin on the grain boundary concurrently, and make the holes or the cracks develop and combine with difficulty, which is a principal factor for improving the creep resistance of the AF15 alloy. The creep resistance of the Al-5Fe-based semisolid alloys at elevated temperature is decreased due to the

accelerated grain boundary sliding generated by the softening of the $\alpha\text{-Al}$ matrix in which the $\theta\text{-Al}_2\text{Cu}$ phase in the alloy is precipitated and coarsened.

CONCLUSIONS

1. The steady-state creep rates of the Al-5Fe-based semisolid alloys increased with increasing temperature and applied stress during tensile creep. The creep resistance of the AF15 alloy is superior to that of the AF1 alloy after adding Cr and Zr elements.
2. There is an inner stress in the Al-5Fe-based semisolid alloys during creep, giving a threshold stress of 14.97 MPa, 19.53 MPa and 20.99 MPa for the AF1 alloys at 300°C, 250°C and 200°C, and of 17.76 MPa, 20.27 MPa and 22.41 MPa for the AF15 alloys at 300°C, 250°C and 200°C, respectively.
3. The creep true stress exponent of the AF1 and AF15 alloys is from 4.34 to 5.34, with average values of 4.88 ± 0.2 and 4.80 ± 0.5 , respectively, close to 5. The creep mechanism of the alloys is dominated by the high-temperature dislocation climb controlled by lattice self-diffusion.
4. Notwithstanding the differences in the creep parameters between the AF1 and AF15 alloys being small, the improved creep resistance of the AF15 alloy is caused by forming larger quantities of more heat-resistant and more compact ring-like or block-like Cr-rich AlFe phases, resulting in the stress concentration decreasing and the micro-holes or the cracks generating and developing with difficulty.

ACKNOWLEDGEMENT

This work is partly supported by Grant No. 21045012513 from Zhejiang Ocean University research start-up funds.

REFERENCES

1. K.E. Knippling, D.C. Dunand, and D.N. Seidman, *Z. Metallkd.* 97, 246 (2006).
2. F. Ji, M.Z. Ma, A.J. Song, W.G. Zhang, H.T. Zong, S.X. Liang, Y. Osamu, and R.P. Liu, *Mater. Sci. Eng. A* 506, 58 (2009).
3. F. Carreño, M. Eddahbi, and O.A. Ruano, *J. Mater. Sci. Lett.* 16, 1728 (1997).
4. B. Liu, X.G. Yuan, and H.J. Huang, *China Foundry* 8, 424 (2011).
5. X.G. Yuan, S.G. Zhao, S. Li, Y.J. Lu, and H.J. Huang, *Foundry* 55, 466 (2006).
6. F. Carreño, M. Eddahbi, and O.A. Ruano, *J. Mater. Sci. Lett.* 16, 1728 (1997).
7. L.M. Peng, S.J. Zhu, H.R. Chen, F.G. Wang, Z.Y. Ma, and J. Bi, *J. Mater. Sci. Technol.* 14, 527 (1998).
8. S. Spigarelli, *Mater. Sci. Eng. A* 337, 306 (2002).
9. K. Kuchařová, S.J. Zhu, and J. Čadek, *Mater. Sci. Eng. A* 355, 267 (2003).
10. L. Pan, F.A. Mirza, K. Liu, and X.-G. Chen, *Mater. Sci. Technol.* 33, 1130 (2017).

11. X.Y. Jiang, Y. Zhang, D.Q. Yi, H.S. Wang, X.B. Deng, and B. Wang, *Mater. Charact.* 130, 181 (2017).
12. J.Y. Zhang, X.Y. Jiang, M.Y. Ma, B. Jiang, B. Wang, and D.Q. Yi, *Mater. Sci. Eng. A* 699, 194 (2017).
13. X.Y. Zhang, H. Zhang, X.X. Kong, and D.F. Fu, *Trans. Nonferrous Met. Soc. China* 25, 1763 (2015).
14. B. Liu, X.G. Yuan, H.J. Huang, and Z.Q. Guo, *JOM* 64, 316 (2012).
15. M.E. Kassner and M.T. Pérez-Prado, *Fundamentals of Creep in Metals and Alloys* (Amsterdam: Elsevier, 2004).
16. M.E. Kassner, *Mater. Sci. Eng.* A410–411, 20 (2005).
17. T. Chen, C.M. Parish, Y. Yang, and L. Tan, *Mater. Sci. Eng. A* 720, 110 (2018).
18. J.S. Zhang, *High temperature deformation and fracture of materials* (Beijing: Science Press, 2007), pp. 90–229.
19. J. Weertman, *J. Appl. Phys.* 28, 362 (1957).
20. B. Liu, *JOM* 67, 3030 (2015).
21. G. Henry and D. Horstmann, *De Ferri Metallographia Band V. Fraktographie und Mikrofraktographie* (Düsseldorf: Stahleisen, 1979).